THE JOURNAL OF PHYSICAL CHEMISTRY B

 VOLUME 106, NUMBER 16, APRIL 25, 2002

LETTERS

Thermodynamic to Kinetic Transition in Epitaxial Electrodeposition

Jay A. Switzer,* Hiten M. Kothari, and Eric W. Bohannan

University of Missouri—Rolla, Department of Chemistry and Graduate Center for Materials Research, Rolla, Missouri 65409-1170

Received: December 20, 2001; In Final Form: March 1, 2002

Ordered nanostructures of cuprous oxide are deposited onto single-crystal gold after a transition from a thermodynamically controlled orientation to a kinetically preferred orientation. Crosshatch patterns of cuprous oxide with a 20 by 100 nm orthogonal nanowire morphology are formed at pH 12 on Au(100). A unique asset of electrodeposition is exploited to deposit these nanostructures: the departure from equilibrium is controlled with millivolt precision by simply selecting an applied electrode overpotential. Small changes in overpotential produce dramatic changes in the morphology of the films. The electrodeposited films follow the [100] orientation of the single-crystal substrate at low overpotential (that is, close to equilibrium) but change to a kinetically preferred [110] orientation at a threshold overpotential of −118 mV. The abrupt change of orientation is triggered by the coalescence of three-dimensional islands that form on the Au(100) surface.

A unique feature of electrodeposition is the ability to control the driving force or departure from equilibrium of the deposition process by simply controlling the applied potential. A variation of a few millivolts can have a profound effect on the morphology of the electrodeposited film. Here, we use this aspect of electrodeposition to produce ordered crosshatch nanostructures of cuprous oxide, Cu_2O, on single-crystal Au. The Cu_2O is deposited onto a Au surface that has a different crystallographic orientation than the preferred orientation that is determined by the kinetics of the process. The departure from equilibrium is determined by the electrode overpotential, η. The overpotential is the difference between the applied potential, E, and the equilibrium potential, E_{eq} (that is, $\eta = E - E_{eq}$). At low overpotential the film will follow the orientation of the substrate indefinitely. At higher overpotential, the film follows the orientation of the substrate (the thermodynamically controlled orientation) until it reaches a critical thickness, after which it switches to the kinetically preferred orientation. Ordered nanostructures are produced on the surface at thicknesses exceeding this critical thickness.

We have previously shown that it is possible to electrodeposit epitaxial films of δ-Bi_2O_3, Cu_2O, ZnO, PbS, and Fe_3O_4 onto single-crystal Au.[1−5] Lincot et al. have electrodeposited epitaxial films of CdTe on InP(111)[6] and ZnO on GaN(0002),[7] while Moffat has produced epitaxial strained-layer Cu/Ni superlattices on Cu(100).[8] In the context of the present paper, these epitaxial films have thermodynamically controlled orientations, because they are determined by the free energy of formation of the films on the single-crystal surfaces. That is, bonds that form between atoms in the film and the substrate control the orientation of the film. It is also well-known in electrochemistry that films will grow with a preferred orientation even on polycrystalline substrates.[9−14] A fiber texture develops, with no in-plane orientation, which corresponds to the fastest growth direction. Amblard et al. have attributed the texture of thick Ni films on polycrystalline substrates to a competitive growth mechanism following grain coalescence. Adsorbed interface inhibitors govern the growth competition leading to a preferred orienta-

* To whom correspondence should be addressed. E-mail: jswitzer@umr.edu

10.1021/jp014638o CCC: $22.00
Published on Web 03/30/2002

TABLE 1: Exchange Current Densities for the Deposition of Cu_2O on the Three Low Index Surfaces of Au at pH 9 and pH 12[a]

	J_0 (A cm^{-2})	
orientation	pH 9	pH 12
[100]	$(7.3 \pm 0.4) \times 10^{-5}$	$(3.0 \pm 0.4) \times 10^{-5}$
[110]	$(4.1 \pm 0.4) \times 10^{-5}$	$(10.5 \pm 0.4) \times 10^{-5}$
[111]	$(2.9 \pm 0.3) \times 10^{-5}$	$(8.5 \pm 0.5) \times 10^{-5}$

[a] The 95% confidence limits for the exchange current densities were calculated using the t-test for 12 measurements at each pH and orientation.

tion.[13] Amblard et al. have also studied the evolution of a [210] texture during the homoepitaxial growth of Ni on Ni(100).[14]

Cuprous oxide is a brick-red, p-type semiconductor with a band gap of 2.1 eV.[2,10] There is evidence that Bose−Einstein condensation of excitons can occur in the material when it is irradiated with high-intensity light.[15−17] Because excitons, like photons, are bosons, they can be made to propagate through a solid coherently. It may be possible to transmit light through an aperture or wire with nanometer dimensions without diffraction losses.[15] The photon can be converted into an exciton, which stores the energy in the electronic state with short wavelength while passing through the aperture, and the exciton can then convert back into a photon on the other side. Although most studies of this effect have been on large single crystals, there is interest in producing nanostructures of Cu_2O, because it may be possible to observe condensation of excitons at lower light intensities. We have also shown previously that layered nanostructures of Cu_2O and Cu can be used to produce a resonant tunneling device that exhibits negative differential resistance at room temperature.[18,19]

Cuprous oxide is ideal for the present study, because the kinetically preferred growth direction is determined by the solution pH. We have previously shown that Cu_2O films deposited on randomly oriented polycrystalline substrates grow with a [100] fiber texture at pH 9 and a [111] fiber texture at pH 12.[11] These films have a strong out-of-plane orientation, but a random in-plane orientation. In the present work, we have measured the growth rates on the various low index faces of Au at pH 9 and pH 12. In electrochemistry, the rate of the electron transfer reaction is directly proportional to the current.[20] For small values of overpotential, η, the Butler−Volmer equation is approximated by

$$J = -J_0 F\eta/RT \qquad (1)$$

where J is the measured current density (A/cm^2), J_0 is the exchange current density (A/cm^2), F is Faraday's constant, η is the applied overpotential (V), R is the molar gas constant, and T is the absolute temperature ($F/RT = 38.92$ V^{-1} at 298 K).[20] The exchange current density, J_0, was determined from the slope of the initial linear regions of linear-sweep voltammograms according to eq 1. The low overpotentials used in these measurements ensured that the film followed the orientation of the substrate. Prior to the measurements a 100 nm thick prelayer of Cu_2O was grown on the single crystals at an overpotential at which the Cu_2O maintains the orientation of the substrate.

Table 1 shows exchange current densities for Cu_2O deposition on each of the low index faces of Au at both pH 9 and at pH 12.[21] The material grows fastest in the [100] direction at pH 9, while at pH 12 it grows fastest in the [110] direction. Notice that J_0 is over 2 times as large in the [100] direction as in the [111] direction at pH 9. At pH 12 the values of J_0 are nearly

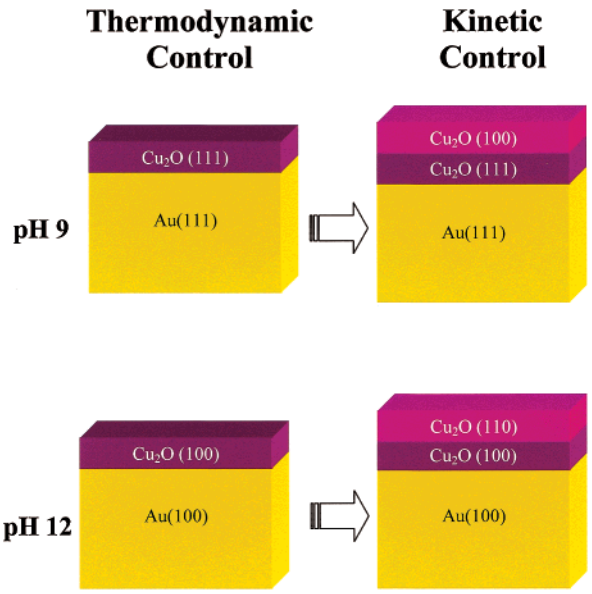

Figure 1. Schematic of the technique used to produce ordered nanostructures of Cu_2O on single-crystal Au. At pH 9 the films are grown on a Au(111) substrate, and at pH 12 the films are grown on a Au(100) substrate. These orientations are not the kinetically preferred orientations. At pH 9 the kinetically preferred orientation is [100], and at pH 12 the kinetically preferred orientation is [110]. After a critical thickness, the films develop these kinetically preferred orientations. At pH 12, a nanometer-scale crosshatch pattern is formed after the [100] to [110] transition.

the same in the [110] and [111] directions, but both of these are approximately 3 times as large as in the [100] direction.

The process we use to produce ordered nanostructures is shown in Figure 1. Cuprous oxide is forced to grow with a [111] orientation at pH 9 on a Au(111) electrode, and with a [100] orientation at pH 12 on a Au(100) electrode. At their respective critical thicknesses, the film on the Au(111) surface changes to a [100] orientation, while the film on the Au(100) surface changes to a [110] orientation. At low η, or close to equilibrium, the film follows the orientation of the substrate for all thicknesses. After a threshold η, the film changes to the kinetically preferred orientation with a critical thickness which decreases as η is increased. The change of orientation produces a surface covered with ordered nanostructures.

Atomic force microscope (AFM) images and X-ray pole figures of films that have undergone the thermodynamic to kinetic transition at both pH 9 and pH 12 are shown in Figure 2. The films are 2000 and 100 nm thick for pH 9 and pH 12, respectively. The critical thickness for the transition at pH 9 ($\eta = -385$ mV) is approximately 200 nm, while at pH 12 ($\eta = -230$ mV) the critical thickness is approximately 10 nm. The AFM image in Figure 2A of the film deposited at pH 9 shows twinned pyramids of Cu_2O that are approximately 520 nm in size. The film grown at pH 12 has a highly ordered crosshatched pattern (see Figure 2B) with orthogonal nanowire-like rectangular features that are approximately 20 nm wide and 100 nm long. The crosshatch pattern is similar to that observed by other researchers during epitaxial growth by molecular beam epitaxy of lattice mismatched layers of cubic semiconductors on [100] oriented surfaces.[22,23] The crosshatch pattern in the semiconductors is reported to be due to strain relaxation associated with misfit dislocation formation and lateral step flow.

The X-ray pole figures in Figure 2C,D show the in-plane and out-of-plane orientation of the films deposited at pH 9 and 12, respectively.[24] Pole figures are run by choosing a diffraction

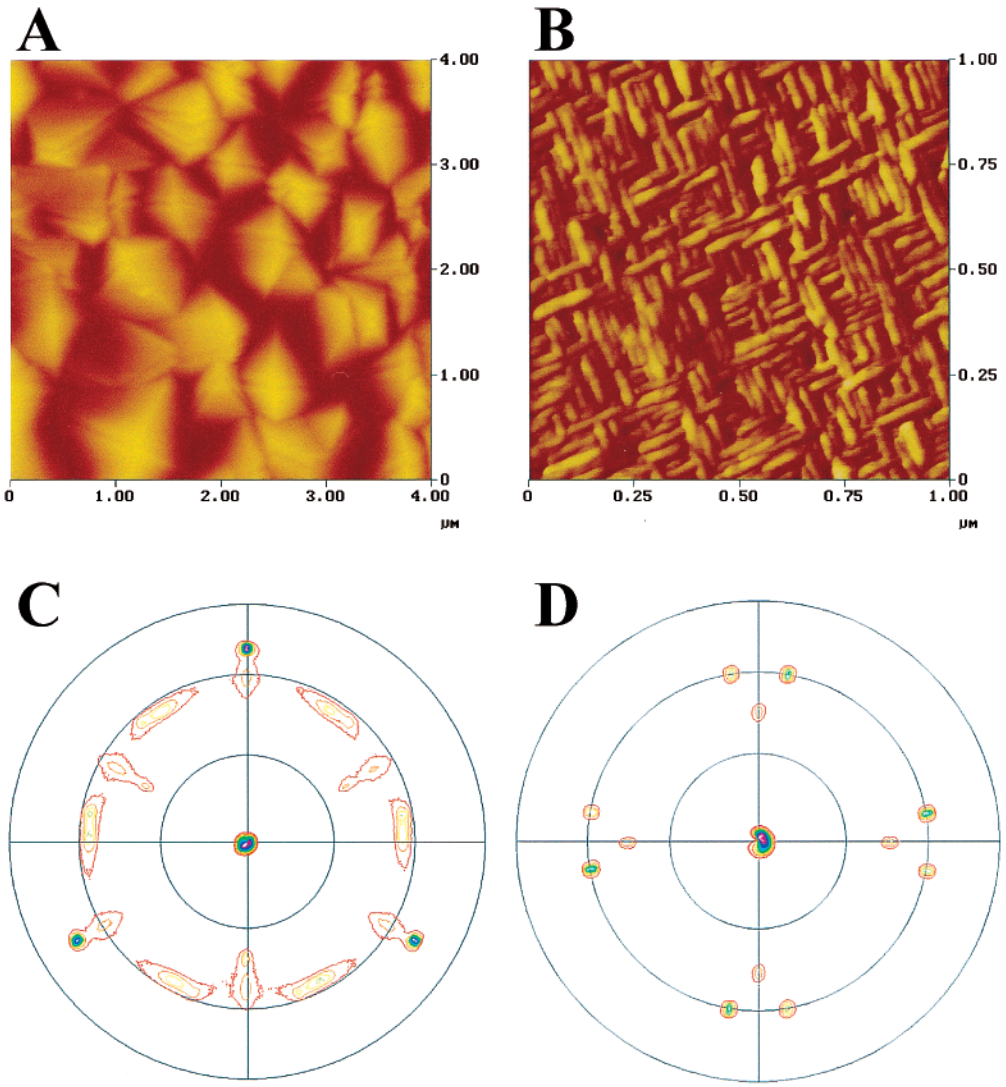

Figure 2. Atomic force microscope images (A, B) and X-ray pole figures (C, D) of films on Au(111) and Au(100) that have undergone the change of orientation. The AFM image in (A) is of a film that is 2000 nm thick that was deposited on Au(111) at pH 9. After undergoing the [111] to [100] transition at a thickness of about 200 nm, the film developed a highly twinned morphology of [100]-oriented grains with dimensions of approximately 520 nm. The AFM image in (B) is of a film that is 100 nm thick that was deposited on Au(100) at pH 12. After undergoing the [100] to [110] transition at a critical thickness of about 10 nm, the film developed a crosshatch nanostructure with orthogonal rectangular features 20 nm wide and 100 nm long. The (111) X-ray pole figure in (C) shows not only the expected [111] and [100] orientations, but also [511] orientations that are produced by twinning of the (111) planes. The (110) pole figure in (D) of the film grown at pH 12 is much simpler. Only the original [100] and the transformed [110] orientations are observed. The radial grid lines on the pole figures correspond to 30° increments in the tilt angle, χ.

angle, 2θ, for a plane that is not parallel with the surface of the material. The tilt of the sample, χ, is then incrementally varied, with the azimuthal angle, ϕ, varied from 0 to 360° at each value of χ. Peaks occur in the pole figure when the Bragg condition is satisfied. The (111) pole figure in Figure 2C of the film grown at pH 9 is complex. It shows three peaks at $\chi = 70°$ separated by $\Delta\phi = 120°$ that correspond to the initial [111] orientation. Only these three peaks are observed if the film does not exceed the critical thickness. Twelve peaks at approximately $\chi = 55°$ separated by $\Delta\phi = 30°$ are due to three equivalent 4-fold symmetric [100] orientations that are rotated 120° relative to each other. In addition to the expected peaks that are due to the [111] and [100] orientations, there are also three peaks at $\chi = 39°$ and six peaks at $\chi = 56°$ (close to the (100) peaks but rotated 7° azimuthally), which are due to the [511] orientation. The observation of these (511) peaks may help elucidate the mechanism of the [111] to [100] transition. Crystallographic twinning of {111} planes is known to produce {511} planes.[25,26] This twinning would be expected to occur from strain that results after coalescence during the nucleation and growth of the [111]-oriented grains. The X-ray pole figure shows that the (511) planes are parallel with the electrode surface. Following Somorjai's treatment, high-index planes with Miller indices (*hkl*) can be described as stepped surfaces according to

$$(hkl) = S - w(hkl)_{\text{terrace}} \text{ x } (hkl)_{\text{step}} \qquad (2)$$

where S indicates a stepped surface, $(hkl)_{\text{terrace}}$ and $(hkl)_{\text{step}}$ are the Miller indices for the terraces and step planes, and w is the number of atoms that are counted in the width of the terrace.[27] For the (511) surface, $(511) = S - 3(100)_{\text{terrace}} \text{ x } (111)_{\text{step}}$. The (100) planes are tilted 15.8° relative to the surface of the electrode. Hence, the (511) surface may provide (100) terraces upon which the [100]-oriented grains can nucleate.

The (110) pole figure in Figure 2D of the film deposited at pH 12 is much simpler. It shows only the (100) peaks at $\chi = 45°$ due to the original orientation, and two orthogonal sets of (110) peaks at $\chi = 60°$ rotated azimuthally ±45° relative to the (100) peaks. Only the four peaks due to the [100] orientation at $\chi = 45°$ are observed if the deposition is run at low

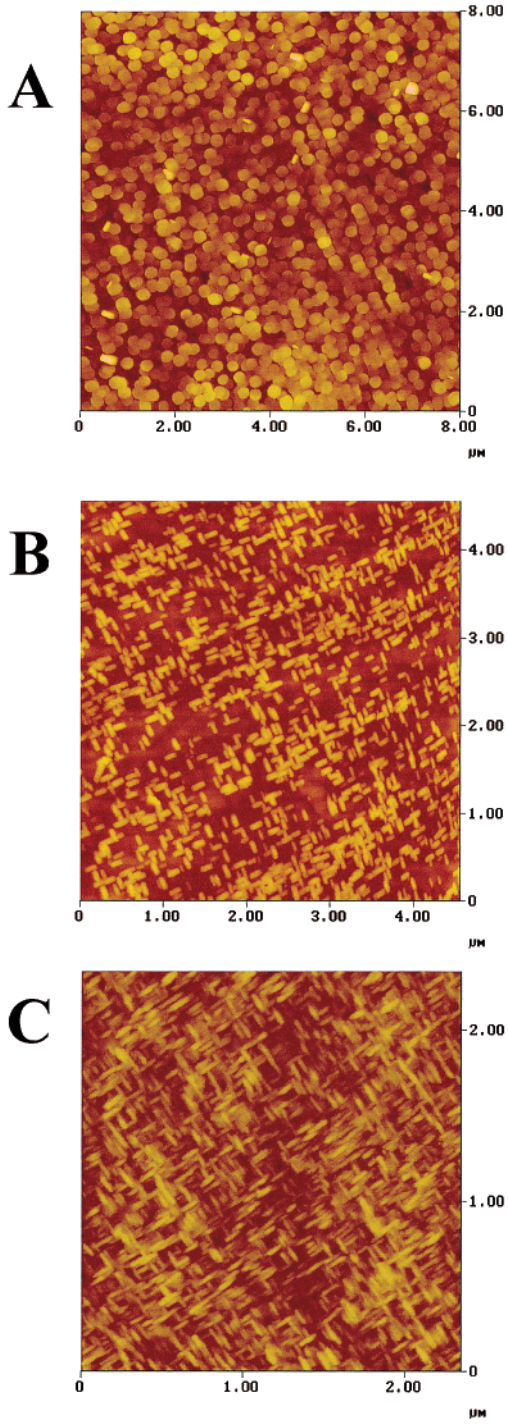

Figure 3. AFM images of three films deposited on Au(100) at pH 12 to a thickness of 100 nm at three different overpotentials. The film deposited at $\eta = -80$ mV (A) follows the orientation of the Au(100). The two films deposited at overpotentials of −118 and −230 mV (B, C) develop the [110] crosshatch pattern. The threshold overpotential for this [100] to [110] transition is −118 mV. The critical thickness at this transition is approximately 25 nm.

overpotential. The transformation occurs very abruptly at pH 12 to form the crosshatch pattern at critical thicknesses in the 10−25 nm range, depending on overpotential.

At low overpotentials Cu_2O does not undergo the thermodynamic to kinetic transition. AFM images of 100 nm thick films deposited at pH 12 onto Au(100) at overpotentials of −80, −118, and −230 mV are shown in Figure 3. The film grown at $\eta = -80$ mV (Figure 3A) consists of uniaxed grains that are approximately 240 nm in size, suggestive of a [100] orientation.

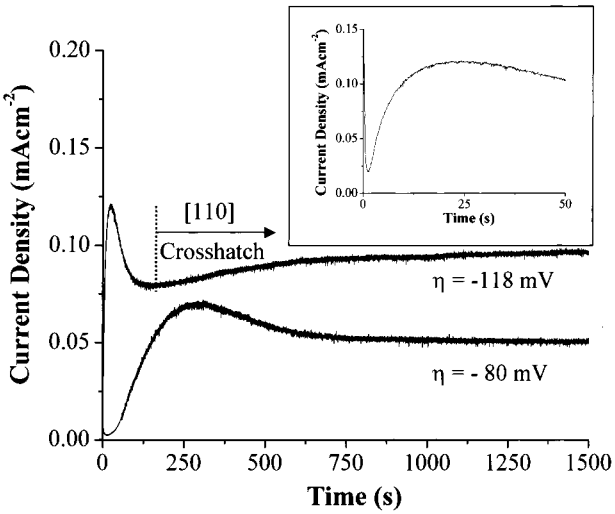

Figure 4. Current−time transients for two films deposited on Au(100) at pH 12 at overpotentials of −80 and −118 mV. Both transients have initial nucleation, growth, and coalescence features for the [100] orientation. The transient for the films deposited at −118 mV has an additional nucleation feature at approximately 125 s and a thickness of 25 nm corresponding to the formation of the [110] crosshatch pattern. The inset shows the current−time transient for the initial period following the potential step for the film grown at an overpotential of −118 mV. The inset illustrates the relatively short induction time for three-dimensional nucleation and growth following the double layer charging.

X-ray diffraction results verify the [100] orientation. The two other films both show [110] crosshatch patterns. The threshold overpotential for this transition is approximately −118 mV. This corresponds to the overpotential at which the rate of the back electron transfer reaction is typically only 1% of the rate of the forward reaction.[20,28] Hence, the system is far from equilibrium, and it is expected that the kinetically preferred orientation would develop.

The critical thickness for the thermodynamic to kinetic transition can be determined from current−time transients that result when the electrode potential is stepped from open circuit to an applied overpotential. The thickness of the film at any time, t, along the transient can be estimated from Faraday's law by integrating from $t = 0$ to t. Current−time transients are shown in Figure 4 for films deposited at overpotentials of −80 and −118 mV on Au(100) at pH 12. We know from the results presented in Figure 3 that the film deposited at $\eta = -80$ mV does not change orientation, while the film deposited at $\eta = -118$ mV develops the [110] crosshatch pattern. Both overpotentials produce transients typical of a three-dimensional nucleation-and-growth mechanism with overlapping diffusion zones.[29,30] A change from progressive nucleation to instantaneous nucleation is observed as the overpotential is changed from −80 to −118 mV. The transients fit the three-dimensional instantaneous nucleation model for all overpotentials more negative than −118 mV. Island growth is expected, because there is a 4.7% lattice mismatch between Cu_2O and Au.[2] At $\eta = -80$ mV the three-dimensional nucleation begins after an induction time of approximately 10 s (thickness = 0.3 nm), and the coalescence of grains occurs after about 250 s (thickness = 22 nm). Following coalescence, the current drops to a steady state. At $\eta = -118$ mV the three-dimensional nucleation occurs (see inset of Figure 4) at 1.3 s (thickness = 0.3 nm), and coalescence of the grains occurs at 25 s (thickness = 5.7 nm). Following the initial coalescence, however, the current does not decay to a steady state like it did at $\eta = -80$ mV. There is a second nucleation step observed at a time of approximately 125

s. We have determined from X-ray diffraction and atomic force microscopy that the film undergoes the [100] to [110] transition during this second nucleation step. The thickness of the film at this transition from [100] to [110] is 25 nm. The increase in current following the initial coalescence can be attributed to the faster growth in the kinetically favored [110] direction, and to the increased roughness of the surface as the crosshatch pattern develops. Films deposited at a lower driving force than $\eta = -80$ mV do not show the second nucleation step, while films deposited at higher driving force than the threshold overpotential of −118 mV all show the second nucleation step, with a critical thickness that decreases as the driving force is increased. The [100] to [110] transition is apparently triggered by strain that develops when the [100]-oriented islands coalesce. If a film that is deposited at an overpotential of −80 mV is allowed to grow to a thickness exceeding coalescence, and is then switched to a higher overpotential like −230 mV, the film orientation does not change. The signature of the transition as well as the critical thickness can, therefore, be determined in real time from these current−time transients.

The orientation of Cu_2O can by tuned by controlling the solution pH or the electrode overpotential. The transition from thermodynamic to kinetic control of orientation was shown in this paper for the specific case of Cu_2O on Au. The phenomenon should, however, be quite general, because kinetically preferred fiber textures are ubiquitous in electrodeposition.[9−14] This technique should also be applicable to the deposition of ordered nanostructures of electronic and magnetic metal oxides onto compound semiconductors such as InP and GaAs.[31]

Acknowledgment. This work was supported by NSF grants CHE-9816484, DMR-0071365, and DMR-0076338 and the Foundation for Chemical Research.

References and Notes

(1) Switzer, J. A.; Shumsky, M. G.; Bohannan, E. W. *Science* **1999**, *284*, 293.

(2) Bohannan, E. W.; Shumsky, M. G.; Switzer, J. A. *Chem. Mater.* **1999**, *11*, 2289.

(3) Liu, R.; Vertegel, A. A.; Bohannan, E. W.; Sorenson, T. A.; Switzer, J. A. *Chem. Mater.* **2001**, *13*, 508.

(4) Vertegel, A. A.; Shumsky, M. G.; Switzer, J. A. *Angew. Chem., Int. Ed. Engl.* **1999**, *38*, 3169.

(5) Nikiforov, M. P.; Vertegel, A. A.; Shumsky, M. G.; Switzer, J. A. *Adv. Mater.* **2000**, *12*, 1351.

(6) Lincot, D.; Kampmann, A.; Mokili, B.; Vedel, J.; Cortes, R.; Froment, M. *Appl. Phys. Lett.* **1995**, *67*, 2355.

(7) Pauporte, Th.; Lincot, D. *Appl. Phys. Lett.* **1999**, *75*, 3817.

(8) Moffat, T. P. *J. Electrochem. Soc.* **1995**, *142*, 3767.

(9) Switzer, J. A.; Shane, M. J.; Phillips, R. J. *Science* **1990**, *247*, 444.

(10) Phillips, R. J.; Golden, T. D.; Shumsky, M. G.; Bohannan, E. W.; Switzer, J. A. *Chem. Mater.* **1997**, *9*, 1670.

(11) Golden, T. D.; Shumsky, M. G.; Zhou, Y.; VanderWerf, R. A.; Van Leeuwen, R. A.; Switzer, J. A. *Chem. Mater.* **1996**, *8*, 2499.

(12) Breyfogle, B. E.; Hung, C.-J.; Shumsky, M. J.; Switzer, J. A. *J. Electrochem. Soc.* **1996**, *143*, 2741.

(13) Amblard, J.; Epelboin, I.; Froment, M.; Maurin, G. *J. Appl. Electrochem.* **1979**, *9*, 233.

(14) Amblard, J.; Froment, M.; Maurin, G.; Spyrellis, N.; Trevisan-Souteyrand, E. *Electrochim. Acta* **1983**, *28*, 909.

(15) Snoke, D. *Science* **1996**, *273*, 1351.

(16) Mysyrowicz, A.; Benson, E.; Fortin, E. *Phys. Rev. Lett.* **1996**, *77*, 896.

(17) Johnsen, K.; Kavoulakis, G. M. *Phys. Rev. Lett.* **2001**, *86*, 858.

(18) Switzer J. A.; Hung, C.-J.; Huang, L.-Y.; Switzer, E. R.; Kammler, D. R.; Golden, T. D.; Bohannan, E. W. *J. Am. Chem. Soc.* **1998**, *120*, 3530.

(19) Switzer, J. A.; Maune, B. M.; Raub, E. R.; Bohannan, E. W. *J. Phys. Chem. B* **1999**, *103*, 395.

(20) Bard, A. J.; Faulkner, L. R. *Electrochemical Methods*; John Wiley & Sons: New York, 2001; Chapter 3.

(21) The films were deposited from aqueous solutions that were 0.4 M Cu(II) and 3.0 M lactate ion, with the pH adjusted to either 9 or 12 with NaOH. The depositions were run in the pH 9 and 12 solutions at 65 and 25 °C, respectively. The Au single crystal substrates were 1 cm in diameter and 2 mm thick. Prior to each deposition, the Au crystals were mechanically polished, electropolished, and then annealed in a hydrogen flame. The equilibrium potentials for cuprous oxide in the pH 9 and 12 solutions were −0.065 and −0.220 V vs SCE, respectively. No corrections were made for the uncompensated resistance.

(22) Andrews, A. M.; Romanov, A. E.; Speck, J. S.; Bobeth, M.; Pompe, W. *Appl. Phys. Lett.* **2000**, *77*, 3740.

(23) Springholz, G. *Appl. Phys. Lett.* **1999**, *75*, 3099.

(24) X-ray pole figures were run on a Philips X-Pert high-resolution diffractometer using Cu Kα radiation. The point-focus primary optics consisted of a crossed-slit collimator, and the secondary optics were a parallel-plate collimator with graphite monochromator. The (111) pole figure was run at $2\theta = 36.441°$, and the (110) pole figure was run at $2\theta = 29.553°$. In a cubic system, the angles between {110} planes and {100} and {110} planes are 45 and 60°, respectively. The angle between {111} and {100} planes is 54.7°, and the angles between {111} and {511} planes are 38.9, 56.3, and 70.5°.

(25) Thomas, G.; Goringe, M. J. *Transmission Electron Microscopy of Materials*; John Wiley & Sons: New York, 1979; p 92.

(26) Tomov, I.; Adamik, M.; Barna, P. B. *Thin Solid Films* **2000**, *371*, 17.

(27) Somorjai, G. A. *Introduction to Surface Chemistry and Catalysis*; John Wiley & Sons: New York, 1994; p 47.

(28) Switzer, J. A.; Hung, C.-J.; Breyfogle, B. E.; Shumsky, M. G.; Van Leeuwen, R.; Golden, T. D. *Science* **1994**, *264*, 1573.

(29) Scharifker, B.; Hills, G. *J. Electroanal. Chem.* **1983**, *28*, 879.

(30) Hölzle, M. H.; Apsel, C. W.; Will, T.; Kolb, D. M. *J. Electrochem. Soc.* **1995**, *142*, 3741.

(31) Preliminary work in our laboratory (Liu, R.; Switzer, J. A. unpublished results) has shown that Cu_2O also develops a [110] crosshatch morphology when deposited at pH 12 onto InP(100).